Stability and Optimality in Bone Remodeling Simulation

Numerical simulations can aid physicians and engineers in studying bone remodeling by indicating which patterns of bone density can be explained by mechanical effects, and which patterns could be due to biological factors. However, the simulations must be numerically robust to offer this service, so that differences between calculated and observed density distributions are not due to numerical artifacts. In this paper, we review some existing bone remodeling theories, then we review a bone remodeling stimulus which we have characterized in some detail. The connection between a particular remodeling rate equation and an optimization process is detailed, and the arguments used to show that the rate equation has a unique steady-state solution are reviewed. The optimization process leads to simple predictions of the behavior of large-scale simulations, and we show that these predictions are borne out.

Key Words: *bone remodeling, computer simulations, stability analysis, prostheses, orthopedics*

INTRODUCTION

Vertebrates have developed the bones of the skeleton in a fairly consistent manner, using bone tissue which varies remarkably little in organization in species as diverse as mice, birds, antelopes, primates, and elephants. The organization of bone has been studied extensively, and several avenues of investigation have shown that mechanical factors are very important to the design of the bony skeleton. Mechanical strain, for example, explains a large amount of variation in the size, shape, and density of bones, as detailed by allometric scaling studies.[52] These scaling

Comments Theor. Biol.
1998, Vol. 5, No. 1, pp. 1–47
Reprints available directly from the publisher
Photocopying permitted by license only

studies are confluent with experimental measurements which show that peak strains in bone are remarkably similar in several species.[4] Further, the seminal work of Wolff[57] showed that estimates of stresses within bones correlate very well with observed trabecular patterns in bone. This feature, and the related claim that bone is optimized to carry the loads on the skeleton with the least amount of mass, led to what is loosely called "Wolff's Law of bone remodeling".

However, there are definite limits to Wolff's law, as can be readily seen in the orthopedic literature. As reviewed by Bertram and Swartz,[5] biological factors can explain many of the findings in bone remodeling experiments where mechanical factors are changed using surgery. This makes it difficult to identify which remodeling responses are due to mechanical or biological factors in these experiments. Controlling the biological factors while manipulating mechanical factors is an experimental goal which is rarely achieved, and until this is regularly achieved, experimental quantification of Wolff's law will be limited by serious questions about biological effects which can mask, imitate, or overwhelm the mechanical effects.

To develop a mechanical relationship which predicts bone remodeling, the behavior of the mathematical model by itself must be carefully studied. This is apparent from the stability problems which have recently been documented in the orthopedic biomechanics literature[18,56] where stability is recognized as a significant problem. If a mathematical model is badly behaved, or is likely to have numerical stability problems, then comparing the results of the model with experimental data is complicated, because the model results could be due to numerical artifact, rather than the relationships in the model. This problem makes many of the current remodeling theories very difficult to apply to experimental or clinical data.

The physical variables used in bone remodeling theories are generally continuum-level measures of stress, strain, elastic properties, and density. Continuum-level properties of any material are averages of the properties over several microstructural dimensions, such as a mean path length in a gas, or the distance between trabeculae in cancellous bone.[17] Given this relationship, the connection between a continuum-level bone remodeling theory and the cellular processes which remodel bone is not well characterized. Attempts to make such a connection are underway, based on homogenization theory[28] and on statistical arguments.[25] A simple connection was shown by Beaupré *et al.*[2] which accounted for stress concentrations within the microstructure by dividing a stress measure by the square of bone den-

sity to estimate stress within the bone microstructure. The connection between continuum-level bone remodeling predictions and the microstructure of bone continues to be a challenge to researchers in this field.

Bone remodeling predictions can be motivated either by a rate equation which predicts local changes due to local variables, or by a global optimization approach, which minimizes an indicator function with respect to parameters which describe the bone structure. Most current remodeling simulations use the rate equation approach, but some work globally. Recently, the two approaches were shown to be equivalent for a restricted class of bone remodeling laws. These will be reviewed in this paper.

The connection between an optimization approach and a remodeling rate equation approach can be likened to the connection between developing dynamic equations from Newton's Laws and using Hamilton's principle. Just as Hamilton's principle depends on the validity of Newton's Laws, the optimization approach to bone remodeling depends on the validity of the rate equation. In this sense, an optimization approach does not address any new physics, but it casts the bone remodeling problem is a manner which allows some very useful simplifications. This allows us to understand the relative influence of the parameters we use in the simulations, and it allows us to show uniqueness and stability in a global sense. These advantages make this remodeling approach robust and stable enough to compare with experimental data, since we can be confident that the remodeling rate equations we use are reflected in the numerical predictions without substantial artifact.

MATHEMATICAL MODELS FOR BONE REMODELING

Several groups of investigators have attemptied to explain the reaction of bone to mechanical stress. The approaches fall into categories based on the mechanical variables used in the remodeling stimulus. The general approach we take to these remodeling theories can be summarized by Figure 1.

In this block diagram, the forces on a bone are inputs to a mechanical system which is a feedback sensor for the remodeling rule. The structural model takes as input the variables which describe the structure (density, shape, and the like) and it produces as an output a stimulus for bone remodeling. The stimulus is compared to a set point, and the error signal is used as an input to the remodeling mechanism. This mechanism generally

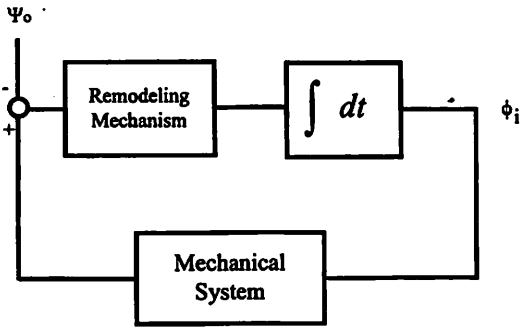

FIGURE 1 A block diagram of bone remodeling: the state variables at right are bone density, and the structural system is characterized as a nonlinear feedback element.

produces a rate of change in the structural variables which is integrated to produce the variables which are input to the structural model. This characterization fits most of the remodeling rules used, at least in a linearized sense. The remodeling mechanism can be as simple as a proportional control, or it can be very complicated, using history integrals, the existing structural variables, and other similar structural measures. Several remodeling rules use a "dead zone" within the controlling block, in which the rate of change of structural variables is zero for a range of error signal.

The stress-based and strain energy-based relationships used in many of these models act entirely at the current time. They are based on the assumption that the rate of change of bone density instantaneously changes with the stress state at a given time, and that the rate of change does not depend on what has happened up to that time. Biological data shows that the cell populations which form and resorb bone take some time (of order days[13]) to respond to stress changes, and that the biological machinery which adds bone usually has to resorb bone first. Thus, the predictions of these models are valid only over fairly long time scales (of order months) in which the dynamics of the cellular machinery can be ignored.

These remodeling rules also assume that the rate of change of stress does not affect the remodeling response. There is clear evidence that the rate of change of loads applied to a bone affects the remodeling response,[53] so this at first seems an oversimplification. However, the strain rates (in microstrain per second) which cause bone to remodel correspond to physiologic loads applied at 3 to 15 Hertz, and bone remodels over the span of weeks or months. Therefore, the remodeling rules we use can

account for rate-sensitive effects by breaking the temporal loading patterns into frequency components, considering the single loading case as a sum of the frequency components, and weighting the high frequency components more heavily than the low-frequency components. This depends on being able to use a linear sum of the stimulus values within the remodeling rule, however, and it is one more assumption which needs to be verified.

Most bone remodeling models treat bone density and bone shape as the variables used in the structural models for bone. However, bone is a well-oriented structure[14] with properties which can be roughly correlated with the orientation of the microstructure. This orientation can be characterized by a second rank tensor.[14,15] The changes in bony orientation with time can be simulated, given a relationship between orientation and mechanical properties.[10,16] This relationship can be used with a remodeling relationship which predicts orientation and density changes with time. However, carefully posing this remodeling theory requires a large number of internal parameters to be specified, and the experimental data which supports a particular value for each of these parameters is rather thin. For example, the coefficients which relate components of the orientation tensor[15] to mechanical properties of bone are based on mechanical test data which is very difficult to perform.

Bone remodeling theories which use an optimality approach have been used in increasing applications, based on the availability of computer software and hardware to conduct the calculations. These models produce a structure which is very similar to that produced by a remodeling rate equation, and which sometimes show the same stability problems. As will be shown below, the solutions for steady-state points of the remodeling rate equations are also the points where an indicator function has zero rate of change. These points are not always minimal or optimal points, and in some cases they are definitely not minimal or optimal.

Cortical Bone

The work of Cowin[9,11,12] on cortical bone has been widely cited as a clear example of remodeling adaptation. By using several simple models for bone changes based on strain, Cowin showed models which adapted to stress changes in a stable sense and which could be correlated with experiments. Hart and Davey[27] also developed a remodeling finite element model which adjusted geometry and density based on stress. These models accounted for changes in the density of newly formed bone as it mineralizes with time. However, the correspondence between the mod-

els used in these studies and experiment depended on choosing a set point for remodeling which varied with position, making a predictive model very difficult.

Cancellous Bone

In cancellous bone, the mechanical variable used is usually either strain energy density or an "energy stress" which is equal to the square root of the product of strain energy density and elastic modulus.[2] These two variables are usually divided by density to a power, to reflect the stress concentrations in the microstructure, and the result is the bone remodeling stimulus. The models of Huiskes *et al.*,[29] Weinans *et al.*,[56] Carter *et al.*,[7] Beaupré *et al.*[2] and Jacobs *et al.*[32] are examples of this type of analysis. These analyses have produced predictions which agree with qualitative results for remodeling, but as Weinans *et al.*[56] and Harrigan *et al.*[18] showed, these remodeling methods can lead to numerical problems. In fact the stepping-off point for the work shown in this review was the data shown by Weinans.[55] In general, stress and strain energy-based remodeling rules have used either "dead zones", as described above, or they have changed the remodeling rule[18] to achieve stability.

A Summary of our Remodeling Rule

The bone remodeling rule used in the studies we have conducted here is based on the usual assumptions for linear elastic finite element modeling of bones, and on two descriptive relationships. They are a structure-property relationship for bone and a remodeling hypothesis. The structure-property relationship is based on experiment, and the parameters are directly derived from experimental data. The remodeling rule is a simple quantification of Wolff's law, as reviewed above, and it has only two adjustable parameters.

We do not change the geometry of the remodeling bone with time at this point. This means that shape changes can only be simulated by letting element densities decrease to zero. This also means that remodeling responses in which the cortex increases in size are not simulated in this scheme. We shall examine the implications of this scheme before adding the extra parameters required to implement shape changes in bone.

Structure-property relationships have been studied in detail for bone, and the volumetric density of calcified tissue seems to be the best single predictor of elastic modulus. As discussed above, orientation effects can

be added to a description of bone elastic modulus, but the description is not substantially better for it, and the number of adjustable parameters (which later need to be justified somehow) becomes unwieldy. For these reasons, we assume isotropy, a material Poisson's ratio that is constant, and a power law relationship between volumetric hard tissue density, ϕ, and elastic modulus,E,[6]

$$E = E_o \phi^n \tag{1}$$

with n the material exponent, usually taken as 3.[6] In these studies, we have taken E_o = 17GPa, n = 3, and the Poisson's ratio as 0.3.

The remodeling rate equation we use is a simple modification of the relationship used previously. In the studies by Huiskes *et al.*[29] and Weinans *et al.*,[55] the remodeling stimulus was strain energy, Ψ, divided by the mass density of the bone tissue, to arrive at a stimulus per unit mass of calcified tissue. In our studies, we use strain energy density divided by the volumetric density of calcified tissue, ϕ, taken to a power m. The difference between this stimulus and a reference value, Ψ_o, is taken as the error signal for remodeling. In our initial studies, the rate of change of density was taken as proportional to this error signal, and time was scaled so that the rate equation was

$$\frac{d\phi}{dt} = \frac{\Psi}{\phi^m} - \Psi_o \tag{2}$$

Here, we do not specify what the remodeling stimulus means. We have left the parameter m adjustable, and we use this simply as a way to account for the magnification of stress within the microstructure. In our studies, we have found a limit on the value of this parameter m which will assure stable and unique solutions for remodeling problems.

Other Well-known Approaches

It is instructive to compare our bone remodeling rate equation to the rate equations used by other groups conducting cancellous bone remodeling simulations. The two most well known groups are the group at Stanford, under Dennis R. Carter, and the group at Nijmegen, the Netherlands, under Rik Huiskes. In our simulations and in the simulations of these two groups, the remodeling rate equations predict a rate of change in density at a point which is a function of the local bone density and the strain energy density. We can compare these three remodeling rate equa-

tions by making contour plots of the remodeling rate as a function of bone density and strain energy density. To accomplish this, we will summarize and simplify the remodeling rate equations used by these groups.

The Standord group[2] uses a remodeling stimulus

$$\sigma = \sqrt{2E\Psi}\,, \tag{3}$$

with σ an energy stress, and Ψ the macroscopic strain energy density. Transduction from a macroscopic to a microscopic stimulus was accomplished by dividing by the square of volumetric density, ϕ, to arrive at a trabeculae-level stress $\sigma_b = \sigma/\phi^2$. The effect of multiple loading cases and cycles was accounted for by an exponentially-based sum which defines the net stimulus as

$$\psi_b = \left(\sum_{i=1}^{N} \sigma_b^m \right)^{1/m} \tag{4}$$

with m an empirical constant. A remodeling simulation was conducted with the rate of change of density defined by

$$\frac{d\Phi}{dt} = C \begin{pmatrix} \psi_b - (\psi_{as} - W) & if & \psi_b < (\psi_{as} - W) \\ 0 & if & (\psi_{as} - W) < \psi_b < (\psi_{as} + W) \\ \psi_b - (\psi_{as} + W) & if & \psi_b - (\psi_{as} + W) \end{pmatrix} \tag{5}$$

in which W is the half width of the "lazy zone" or "dead zone" and Ψ_{as} is a set point. This approach was used by Beaupre *et al.*[3] to assess remodeling around a total hip replacement. By considering a single load case, and noting that $E = E_o \phi^3$ the remodeling stimulus ψ_b can be rendered as

$$\frac{\psi_b}{\sqrt{2E_o}} = \sqrt{\frac{\Psi}{\phi}} \tag{6}$$

and a normalized rate equation can be implemented by dividing the rate of change by C ψ_{as} and by taking the normalized strain energy density as $2\Psi E_o/\psi_{as}^2$ A contour plot of the normalized rate equation is shown in figure 2 with $W/\psi_{as} = 0.1$, as used by Beaupre.[3]

The bone remodeling scheme used by Huiskes *et al.*[31] uses strain energy density divided by density as the remodeling stimulus, and accounts for multiple loads by simply summing their effect, so that their stimulus S is given by

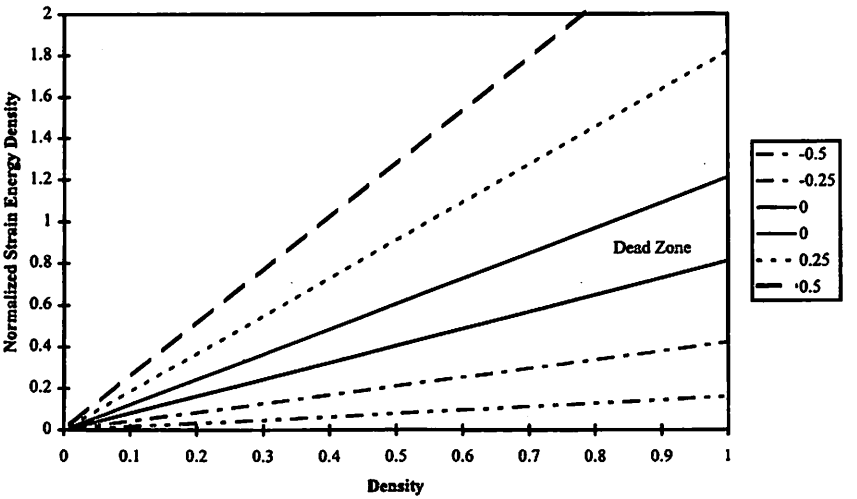

FIGURE 2 A contour plot of the remodeling rate versus strain energy density and volumetric density in the Stanford model. The lines show values of the scaled remodeling stimulus, and the "dead zone" is the region between the two solid lines. Comparing to Figure 3 shows that for a single loading case, the dead zone for the Stanford model and the Nijmegen model can be made identical.

$$S = \frac{1}{n}\sum_{i=1}^{n}\frac{\Psi_i}{\rho} \tag{7}$$

with ρ the apparent density of the cancellous bone, so that $\rho = \phi\rho_b$ with ρ_b the density of calcified bone tissue. The subscript (i) refers to each of several load cases, and as above, Ψ_i is the strain energy density per unit (total) volume in load case number (i). The multiple load stimulus has a "dead zone" (of half-width s) associated with it, and the rate of change in density is also taken as proportional to the available surface area within the microstructure, using a function $a(\rho)$ to give

$$\frac{d\rho}{dt} = a(\rho)\begin{pmatrix} S-(1-s)S_{ref} & if & S<(1-s)S_{ref} \\ 0 & if & (1-s)S_{ref}<S<(1+s)S_{ref} \\ S-(1+s)S_{ref} & if & S>(1_s)S_{ref} \end{pmatrix} \tag{8}$$

and if, for the sake of comparison, we take $a(\rho) = 1$, a single load case, and multiply by ρ_b/S_{ref} then we can make a contour plot of the normalized

rate of change given by this model as a function of Ψ and ϕ, with s = 0.3. Notice from the equation above that the steady-state solution of this remodeling simulation will be within the lazy zone regardless of the choice for a(ρ). This is given in figure 3 and it has a striking similarity to the figure for the Stanford group. This is not surprising, since the remodeling rate depends on the ratio Ψ/ϕ in both formulations, and the straight lines shown in the figures show constant values of this ratio.

Our bone remodeling stimulus is adapted from the remodeling stimulus used extensively by the group in Nijmegen, the Netherlands. The difference in the remodeling rate equation is in an exponent used in the denominator, and the lack of a "lazy zone". The effect of multiple loads is given by

$$S = \sum_{i=1}^{N} \alpha_i \frac{\Psi_i}{\Phi^m} \tag{9}$$

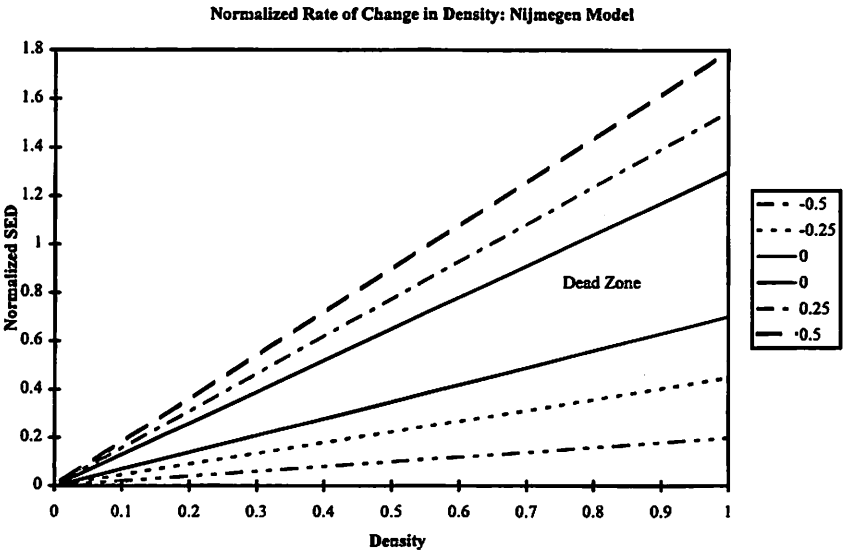

FIGURE 3 A contour plot of the remodeling rate versus strain energy density and volumetric density in the Nijmegen model. The lines show values of the scaled remodeling stimulus, and the "dead zone" is the region between the two solid lines. Comparing to Figure 2 shows that for a single loading case, the dead zone for the Stanford model and the Nijmegen model can be made identical.

and this stimulus is used as described in detail above. Taking $N = 1$, $\alpha_1 = 1$, and dividing by Ψ_0 gives a normalized rate of change as shown in figure 4 with $m = 3.1$. Notice that, for a range of density, the zero line in our simulations is within the "dead zone" in the stimulus for both the Stanford and the Nijmegen group. The range of density in which our zero point is within the dead zone of either group depends on the relative choice of parameters in the models. This shows that our remodeling stimulus gives a steady-state solution which is very similar to the solution which would be obtained with each of these groups.

In general, these results are not especially surprising, because the general formulation of Wolff's law should yield an equilibrium relationship which describes bone density increasing as stress (or some measure of stress) increases. These three laws all adhere to that general property.

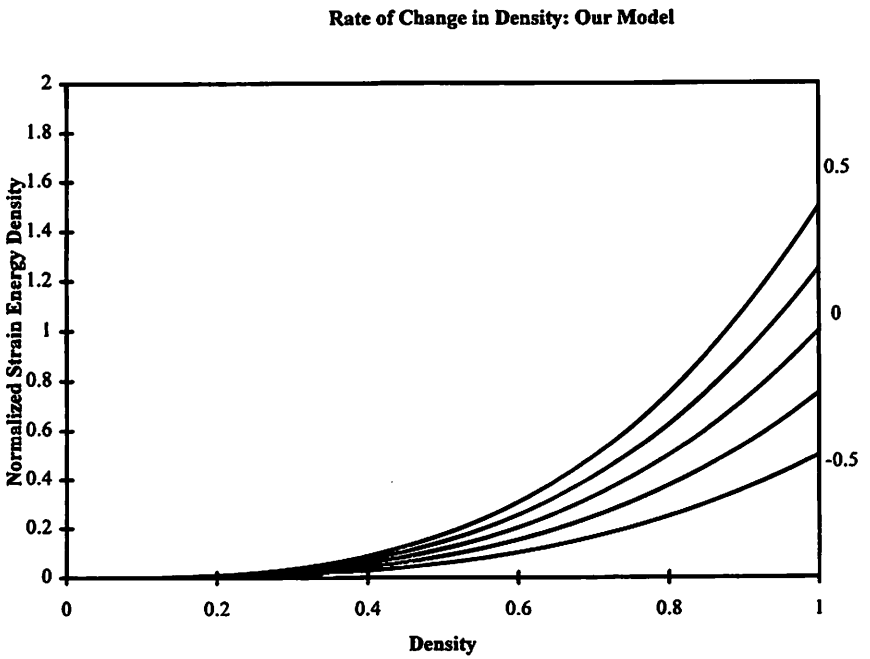

FIGURE 4 A contour plot of the remodeling rate versus strain energy density and volumetric density in our model. The values of scaled remodeling rate are 0.5 (top), 0.25, 0, −0.25, and −0.5 (bottom). Comparison to Figures 2 and 3 shows that for the right choice of parameters, the zero rate of change line is within the "dead zone" of the Nijmegen or Stanford models for a range of densities.

Stability in a Finite Element Implementation

The finite element implementation of these rate equations was carried out by using the usual methods for displacement-based finite element analysis and the direct stiffness method.[1] By carefully using the relationships in finite element modeling, we can cast the entire remodeling problem in terms of the density distribution.

The usual formula for the stiffness of a linear elastic volumetric finite element is

$$L = \int_V B^T C B dV \tag{10}$$

with B the strain-displacement matrix, and C the stress-strain matrix, and the integral carried out numerically over the volume of the finite element. In isotropy, each nonzero component of the stress-strain matrix is proportional to the elastic modulus, so that, from above, each nonzero component is proportional to ϕ^n. If we take the volumetric density as constant within a finite element, this results in an element stiffness matrix in a finite element formulation that we can express as[1]

$${}^e L_{fg} = \phi_e^n {}^e K_{fg} \tag{11}$$

with the left superscript e indicating the element, ${}^eL_{fg}$ the element stiffness matrix and ${}^eK_{fg}$ the element stiffness matrix for unit density. Using this notation, we can write the total stiffness matrix for a finite element model in terms of element densities as

$$K_{fg} = \sum_{e=1}^{N} \phi_e^n {}^e K_{fg} + {}^c K_{fg} \tag{12}$$

with ${}^cK_{fg}$ the non-remodeling part of the finite element matrix.

The average strain energy density within the element, ${}^e\Psi$, for a given displacement solution u is

$${}^e\Psi = \frac{\phi_e^n u_f {}^e K_{fg} u_g}{2V_e} \tag{13}$$

with V_e the element volume.

As above, we use this strain energy density divided by ϕ^m as the remodeling stimulus.

Equation (2) leads to a bone remodeling rate equation which is

$$\frac{\partial \phi_e}{\partial t} = \frac{\phi_e^n u_f {}^c K_{fg} u_g}{2 V_e \phi_e^m} - \Psi_o \tag{14}$$

with Ψ_0 the stimulus set point.

We initially tested this finite element scheme numerically using an Euler forward time stepping scheme, which resulted in stable simulations of several simple problems, and which remained stable as the finite element mesh was refined.[20] However, in some problems, the Euler forward scheme resulted in simulations which exhibited "hunting" behavior and which did not converge. To assess whether there was a stability problem associated with the finite element formulation per se, or with the Euler forward method, we conducted a stability analysis, using perturbations of density, which resulted in the following equation for increments in density:

$$\frac{\partial(\Delta\phi_e)}{\partial t} = M_{es}\Delta\phi_s + D_{es}\Delta\phi_s \tag{15}$$

with

$$M_{es} = \frac{-n\phi_e^{n-m}\phi_s^{n-1} u_f {}^c K_{fp} K_{pq}^{-1} {}^s K_{qg} u_g}{V_e} \tag{16}$$

and

$$D_{es} = \delta_{es} \frac{(n-m) u_f {}^c K_{fg} u_g}{2 V_e} \phi_e^{n-m-1} \tag{17}$$

with δ_{es} equal to 1 if e = s, and zero otherwise.

Since this was a linearized version of the full nonlinear equations, we could use an exponential solution for the behavior of the perturbations with time. These exponential perturbations will all decrease with time if all of the eigenvalues of $M_{es} + D_{es}$ are negative. To test this condition, we instead tested the negative of this matrix for positive definiteness, and we used two facts from matrix theory. First, the symmetric part of a non-symmetric matrix is stable if and only if the matrix itself is stable[51] and second, if a symmetric matrix is triangularized using $K = L\Lambda L^T$ (as in standard finite element equation solvers) then the matrix is positive definite if (and only if) all the terms in the diagonal matrix Λ are positive.

The fact that the matrix $M_{es} + D_{es}$ is not symmetric led to an investigation of whether the matrices could be cast in a symmetric fashion.[19] If

a formulation could be found which made these matrices symmetric, then an optimization approach is possible, since then a reciprocity condition would exist. A reciprocity condition implies that the rate equations are derived from a potential function, and that conditions which make the rate equation zero are conditions which extremize the potential function. These extremum points are then candidates for minimum points.

Finding a state variable which allows the remodeling rate equation to be part of an optimizing process is analogous to finding an energetically conjugate variable in an energy-based approach to a mechanics problem. The analogies between this approach and the use of Hamilton's principle are summarized in figure 5. In Hamilton's principle, an energy function is developed, and generalized displacements are chosen. Generalized forces are given by the derivative of the energy function with respect to the generalized displacements, and this results in reciprocity conditions.

In a recent paper[19] we showed that changing the state variable used in the remodeling equation allows that equation to be a part of an optimizing process. By using density to the power m (the exponent in the denominator of equation 2) we can define a variable γ as

$$\gamma = \phi^m \tag{18}$$

and by taking the rate equation as

$$V^e \frac{\partial \gamma_e}{\partial t} = \frac{\gamma^{\frac{n-m}{m}} \left(u_f{}^e K_{fg} u_g \right)}{2} - \Psi_o V_e \tag{19}$$

	Hamilton's Principal (statics)	Bone Remodeling
Variational Indicator	P=Potential Energy	$H=TSE + \int \gamma \, dv$
Generalized displacements	ξ_i	$\gamma_i=\phi_i^m$
Generalized Forces	$G_i=\partial P/\partial \xi_i$	$F_i=\partial H/\partial \gamma_i=[SED/\phi_i^m]-\Psi_o$
Reciprocity Condition	$\partial G_i/\partial \xi_j=\partial G_j/\partial \xi_i$	$\partial F_i/\partial \gamma_j \;\; \partial F_j/\partial \gamma_i$

FIGURE 5 Comparison between Hamilton's principal (for statics) and the remodeling approach used in these simulations.

we can satisfy the requirements for an optimizing function, because reciprocity holds. We have shown that this remodeling rule gives the same steady state density distributions as the original remodeling rate equation above.

By analogy to Hamilton's principle, as in figure 5, finding a variable γ which satisfies reciprocity conditions is interesting, but to use an optimization approach in general, we need to identify the function which is optimized. We have also shown that finding a distribution of γ which makes the rate of change in eq. 26 zero is equivalent to finding stationary points in the function

$$H = \left(\frac{m}{n}\right) H_1 + H_2 \tag{20}$$

with

$$H_1 = \sum_{e=1}^{N} \frac{u_f \left(\gamma_e^{\frac{n}{m}} {}^e K_{fg} + {}^c K_{fg} \right) u_g}{2} \tag{21}$$

the strain energy in the entire structure, and

$$H_2 = \Psi_o \sum_{e=1}^{N} V_e \gamma_e \tag{22}$$

the integral of γ over the remodeling elements. Notice that H_2 is not proportional to the total mass of calcified tissue.

The optimization function H can be used to prove that there is only one solution to the remodeling equations if $n < m$, and to show that the solution is always stable in this case. It can also be used to show that if $n > m$, no stable solution exists.[23] If we consider the rate equations as

$$V_e \frac{\partial \gamma_e}{\partial t} = -\frac{\partial H}{\partial \gamma_e} = F(\gamma_e) \tag{23}$$

with H defined as $(m/n)H_1 + H_2$, then equation 28 results.

Note that these partial derivatives are taken with a fixed load—*not fixed displacements*. Physically, a change in density at constant load (the mechanically relevant situation here) will change the displacements within the model, so the proper application of this derivative incorporates the chain rule, by using a derivative of H with respect to

displacements, and the derivative of displacements with respect to density. This is detailed in a prior publication.[23]

If we take derivatives of F with respect γ, we can write a perturbation equation which can be written as

$$V_e \frac{\partial(\delta\gamma_e)}{\partial t} = -(T_{es} + P_{es})\delta\gamma_s \tag{24}$$

with

$$T_{es} = \delta_{es}\left(\frac{m-n}{2m}\right)\gamma_e^{\left(\frac{n-2m}{m}\right)}\left(u_f{}^e K_{fp} u_p\right)$$

$$P_{es} = \left(\frac{n}{m}\right)\gamma_e^{\left(\frac{n-m}{m}\right)}\left(u_f{}^e K_{fp} K_{pq}^{-1} u_g\right)\gamma_s^{\left(\frac{n-m}{m}\right)} \tag{25}$$

and in a recent paper we have shown that $T_{es} + P_{es}$ is positive definite for all possible distributions and loading conditions if and only if $n < m$. This in fact proves that the long-term density distribution which solves equation 19 is unique and that eq. 19 is stable.[23]

In summary, a remodeling rate equation which uses strain energy density, divided by density taken to a power m, will always give a stable and unique long-term solution if m is large enough. This shows that a finite element simulation using this rate equation will give numerical results which are robust and unique, and which reflect the remodeling rate equation without numerical artifacts. This remodeling simulation method also follows an optimization scheme which can be very useful as a way to understand the results of remodeling simulations.

Stability Considerations in Other Finite Element Models

As reviewed above, stability considerations have been addressed by the Nijmegen group and the Stanford group, but not in the detail shown above. Generally, simplified models of remodeling, with the stimulus applied to one or two remodeling elements, have been used, and these models have shown surprisingly useful results. However, for a more general approach, we have considered more complicated models.

As mentioned above, the remodeling rate equation we use can be made equivalent to the equation used by the Nijmegen group, by taking the dead zone width equal to zero, using $a(\rho) = 1.0$ and by taking our exponent m equal to unity. With these identifications, the results shown

above all hold regarding optimality, and the optimizing function. In summary, the model used by the Nijmegen group optimizes a weighted sum of the total mass in a structure and the total strain energy stored in it (including prostheses). However, the analysis also shows that simple rate equations, such as studied here, are unstable at a continuous solution for density. This means that if the stimulus used by the Nijmegen group is operative in the natural case, then the dynamic processes which bring about continuous density distributions in natural bones are fairly complex.

Stability in the models used by the group at Stanford have been investigated by numerical experiments in which changes in the temporal relationships were assessed,[33] and by experiments in which continuity constraints are placed in the density distribution, using finite element techniques.[32] An analytical investigation of the stability of these methods (i. e. linearizing and studying the character of the linearized equations) is nearly impossible, since the relationships used are very complex. Clearly, with a dead zone used, there is not a unique solution, but if a dead zone is not used, it remains to be seen whether the formulation used by the Stanford group can be put into a form which has an optimizing character. Also, it is not clear whether certain parameter choices or load cases can make the simulations stable.

With a dead zone width taken as zero, the Stanford model becomes

$$\rho_c \frac{d\phi_b}{dt} = C\left[\phi_b^{-2}\left(\sum_i \sqrt{2E_b{}^i\Psi_b}\right)^{1/m} - \Psi_{at}\right] \tag{26}$$

with ρ_c the density of fully calcified tissue, the superscript i denoting a particular load case, and the subscript b denoting a certain (discretized) value of volumetric density ϕ or strain energy density Ψ. By using $E_b = E_o\phi^z$ and rearranging terms, we can re-write this more clearly as

$$\frac{\rho_c}{C\sqrt{2E_o}}\frac{d\phi_b}{dt} = \phi_b^{\frac{z}{2}-2}\left(\sum_i \left({}^i\Psi_b\right)^{\frac{m}{2}}\right)^{1/m} - \frac{\Psi_{at}}{\sqrt{2E_o}} \tag{27}$$

and we can now discuss how the problem is discretized and linearized. If a finite element formulation is used, and if density is assumed constant in each element, as above, then we can proceed as above, by relating strain energy density to volumetric density and nodal point displacements via the element stiffness matrices. If density is allowed to vary within an element, then the situation is not as clear. However,

if we remember the way strains are related to nodal point displacements in a finite element, then varying density within an element is not a large conceptual leap. Local stiffness matrices in finite elements are evaluated using Gaussian quadrature by a summation which is essentially (for 3D elements)

$$K_{ij} = \sum_{r}^{n_g} w_r \sum_{s}^{n_g} w_s \sum_{t}^{n_g} w_t \; B_{if}(\xi_r, \xi_s, \xi_t) C_{fg}(\xi_r, \xi_s, \xi_t) B_{gi}(\xi_r, \xi_s, \xi_t) \det J \quad (28)$$

with w_i the Gaussian weights and ξ_r the gaussian weighting points, $B_{ij}(r,s,t)$ the position-dependent matrix which relates displacements to strain, $C_{ij}(r,s,t)$ the stress-strain matrix, and det J the determinant of the jacobian between the local coordinate system and the global coordinate system. Allowing density to vary within the element is the same as allowing the matrix C to vary. In forming the finite element stiffness matrix, these matrices are evaluated at specific points in the finite element. Since these matrices are available during a structural analysis, it is a simple matter to calculate the strain energy density at a point as

$$\Psi(r,s,t) = (1/2)\, u_i \; B_{if}(r,s,t) C_{fg}(r,s,t) B_{bj}(r,s,t) u_j \quad (29)$$

and the strain energy density at a given point can be assessed easily. If the points where the strain energy density are evaluated are the Gaussian integration points, then the total stiffness matrix can be written in terms of those points, by inserting the formula for each matrix into the formula for the total stiffness matrix. This will allow one to calculate the derivative of displacements in the mesh with respect to density at a given gaussian integration point, and a stability analysis can proceed as above.

The strain energy density at any point in the model must be positive, since the material matrix C is positive definite, so exploring stability in a remodeling simulation which allows density to vary within an element is similar to exploring stability in a remodeling simulation which assumes the density is constant within elements. In fact, if there were substantial differences, then the results would be suspect, since the stability of the overall simulation would depend on the approximations used to solve the continuum-level equations.

Nodal point-based bone remodeling formulations differ from element-based formulations in the way that strain energy density, calcu-

lated within an element, is related to a value of strain energy density used at a nodal point. From basic considerations in finite element modelling, the strain energy density which would be estimated by two finite elements at a point on their common boundary will in general be different, and the difference will become close to zero as the element size shrinks to zero. This means that a given node in a node-based remodeling simulation will have two or more estimates of stress or strain energy density from the elements which it is used in. Averaging these estimates is reasonable, but that process couples adjacent elements in ways which are not easily understood. However, as element size shrinks, and the differences in stress estimates decrease, the formulation should produce results which do not depend on the averaging process.

An analysis of the remodeling method used by the Stanford group (taking density as constant within an element) indicates that the remodeling approach used does not fit into an optimization scheme, at least along the lines that our remodeling algorithm does. The primary difficulty is in the summation scheme for multiple loads. Writing the strain energy density (for load i) in an element as

$$ {}^{i}\Psi_b = {}^{i}u_r \left(\phi_b^{z\,b} K_{rs}^{o} \right) {}^{i}u_s \tag{30} $$

with ${}^{i}u_s$ the displacement component number s due to load i, and ${}^{b}K^{o}_{rs}$ the stiffness matrix for element "b" at unit volumetric density. Taking density out of the summation gives

$$ \frac{\rho_c}{C\sqrt{2E_o}} \frac{d\phi_b}{dt} = \phi_b^{z-2} \left(\sum_i n_1 \left({}^{i}u_r \, {}^{b}K_{rs}^{o} \, {}^{i}u_s \right)^{\frac{m}{2}} \right)^{1/m} - \frac{\Psi_{at}}{\sqrt{2E_o}} \tag{31} $$

And if we substitute $\chi_b = \phi_b^2$, using the wisdom accrued above, we have

$$ \frac{\rho_c}{C\sqrt{2E_o}} \frac{d(\chi_b)^{1/2}}{dt} = \chi_b^{\frac{z}{2}-1} \left(\sum_i n_1 \left({}^{i}u_r \, {}^{b}K_{rs}^{o} \, {}^{i}u_s \right)^{\frac{m}{2}} \right)^{1/m} - \frac{\Psi_{at}}{\sqrt{2E_o}} = F_b \tag{32} $$

Taking direct partial derivatives with respect to χ_b and indirect derivatives (via the chain rule using displacements) with respect to χ_p as above, (also assuming that load is constant with time) yields.

$$\frac{\partial F_b}{\partial \chi_p} + \sum_h \frac{\partial F_b}{\partial {}^h u_k}\frac{\partial {}^h u_k}{\partial \chi_p} = \delta_{pb}\left(\frac{z}{2}-1\right)\chi_b^{\frac{z}{2}-1}\left(\sum_i n_1\left({}^i u_r\, {}^b K^o_{rs}\, {}^i u_s\right)^{\frac{m}{2}}\right)^{1/m}$$

$$+ \chi_b^{\frac{z}{2}-1}\chi_p^{\frac{z}{2}-1}\left(\sum_i n_i\left({}^i u_e\, {}^b K^o_{ef}\, {}^i u_f\right)^{\frac{m}{2}}\right)^{\frac{1}{m}-1} \times \sum_h\left(n_h\left({}^h u_r\, {}^b K^o_{rs}\, {}^h u_s\right)^{\frac{m}{2}-1}\right)$$

$$\left({}^h u_g\, {}^b K^o_{gk}\left(-K^{-1}_{kq}\right)^p K^o_{qt}\, {}^i u_t\right) \quad (33)$$

Examining the terms in this equation from top to bottom, the left hand side of this equation reflects the chain rule, as applied above to our remodeling simulation. The second term down shows the result of a direct partial derivative with respect to χ_b. The third and fourth terms show the result of a derivative with respect to each component of displacement, followed by a derivative with respect to χ_b and summed. While the term in the right-hand parentheses of the bottom term is symmetric with respect to p and b, the term multiplying it depends only on b, and the third term down (in parentheses) also only depends on b. Thus, while the remodeling rate equation used by the Stanford group may reflect an optimization procedure in some sense, there seems to be no connection analogous to the one used in our remodeling algorithm.

PRACTICAL RESULTS OF AN OPTIMIZATION APPROACH

The key practical advantage of the optimization approach is in the methods for approximate solution which are available from analytical mechanics. By making coarse approximations to the actual solution for a given remodeling problem, the effect of the remodeling parameters on the overall solution can be directly shown. These coarse approximations, shown below, allow analytical solutions for overall trends which are very useful in understanding the physical implications of the remodeling parameters.

In the optimization approach, density patterns are used to compute a value for H, and a restricted set of approximate density patterns can be used for analysis. By finding the density pattern within that restricted set which minimizes H, we can arrive at an approximate solution for the final density pattern. For example, in the finite element procedures we use, the restricted set of density patterns consists of the elements in the mesh, with a uniform (but variable in time) density in each element. That

is, we have used a patchwork of densities based on the finite element mesh. By using a restricted set of density patterns, we can reduce the functional we have found to a function of one or several variables which characterize the density distributions we use. By minimizing the resulting function with respect to the variables which characterize the density distribution, we are finding the density distribution within the restricted set which best minimizes the functional we have developed.

APPLICATION TO INTRAMEDULLARY IMPLANTS

Many studies have shown a drastic loss of bone around uncemented total hip replacements. Porous-coated intramedullary rods, and fiber-reinforced composite materials are proposed as a way to decrease the stiffness of a prosthesis enough to maintain bone. Using the function H described above, we can make a simple prediction of the needed prosthesis size and material stiffness to maintain bone around the implant.

Axial Loads

If we consider a section of bone containing a prosthesis and we assume that the strain within the section is uniform, we can write H as

$$H = \left((m/n)\left(E_p A_p + E_b A_b\right)\left(\epsilon^2/2\right) + \Psi_o A_b\right) L \tag{34}$$

with E_p and E_b the elastic moduli of prosthesis and bone, respectively, A_p and A_b the cross sectional areas of prosthesis and bone, respectively, and L the length of the section. We can now minimize the function H with respect to bone area, and arrive at a prediction of the stem stiffness required to maintain bone adjacent to the stem.

On first glance, this analytical procedure seems to be a geometrical optimization, rather than a density-based optimization, but the density-based optimization is actually general enough to include this type of optimization as a subset. In terms of the remodeling rule we have developed above, this analytical procedure corresponds to choosing a restricted class of density distributions in the optimizing process. That is, we use density distributions which are fully dense (i. e. $\gamma = 1$) over a bone A_b and zero outside that area. This is a subset which is included in the set of all possible density distributions. Thus minimizing H with respect to bone area fits within the framework developed for density—based

remodeling if we consider only density distributions which are a restricted subset of all possible bone density distributions.

Substituting for the strain in terms of the total force on the section yields

$$H = \frac{(m/n)F^2 L}{2(E_p A_p + E_b A_b)} + \Psi_o A_b L \tag{35}$$

Since this is the strain energy only in a section of the structure, we can not expect that minimizing H by manipulating A_b will give an exact answer, but since most femoral prostheses contain long stems, we expect this representative section to allow us to make an approximate generalization. Minimizing H with respect to A_b yields a simple equation for A_b, and for A_b to be greater than zero, we must have

$$E_p A_p < F\sqrt{\frac{mE_b}{2n\Psi_o}}. \tag{36}$$

This requirement can allow us to give a limit on the axial stiffness of an implant to maintain cortical bone around the shaft. Conversely, the limit on the value of Ψ_o needed for maintenance of a cortex is

$$\Psi_o < \left(\frac{F}{E_p A_p}\right)^2 \left(\frac{m}{2n}\right) E_b . \tag{37}$$

These requirements are reflected in the results of the simulations in which the cortex is allowed to remodel.

Transverse Bending Moments

We developed two simplified models for bone adaptation to an intramedullary implant under a transverse bending moment in this study. Both models were aimed at assessing conditions for bone to remain around the implant. The models assumed that the bending radius of curvature for the implant and the surrounding bone were the same, and that bone exists in a concentric ring around an implant, with an interior radius r_i and an exterior radius r_e concentric with the implant section which is characterized by the flexural rigidity $E_p I_p^b$. The inner bone radius is not constrained to be the same as the outer implant radius, since in many clinical cases the bone does not touch the implant in a given cross section.

Given this geometry and an equal radius of curvature for bone and implant, we can write the strain energy of the implant and prosthesis as

$$TSE = \frac{2M^2L}{\pi E_b\left(r_e^4 - r_i^4\right) + 4E_pI_p^b} \tag{38}$$

with M the transverse bending moment and E_b the bone elastic modulus. Both approximate approaches used this expression for total strain energy in the bone and implant. This neglects end effects, but was chosen with the specific purpose of assessing bone maintenance around an intramedullary stem.

In the first optimization model we used, the density of the bone was taken as 1.0 and thus the restricted set of density distributions used in the analytical model consisted of circularly symmetric regions of fully dense bone, with the outer radius taken as fixed, and the inner radius variable. Thus the index which selects the density distribution in the optimization model is r_i—the inner bone radius. Minimizing the indicator functional over this restricted set of bone densities leads to the following equation:

$$\left(\frac{mM^2E_b}{4n\Psi_o}\right)^{1/2} \quad r_i = \frac{\pi E_b}{4}\left(r_e^4 - r_i^4\right) + E_pI_p^b \tag{39}$$

and to assess when cortical bone will be adjacent to the implant, we need to assess the limit as r_i approaches r_e. In that case, the bone flexural stiffness becomes small, and we can replace the first term on the right with ϵ and solve for r_i. For cortical bone to remain around the implant, we require $r_i < r_e$ and this results in

$$E_pI_p^b + \epsilon < r_e\left(\frac{mM^2E_b}{4n\Psi_o}\right)^{1/2} \tag{40}$$

and we can take the limiting value $\epsilon = 0$. This results in a limiting value of flexural stiffness for an intramedullary implant for maintenance of bone, using the single-parameter restricted set of density distributions.

In the second analytical optimization model we used the same geometric analysis but we took volumetric density as a fixed value less than unity. This resulted in the limit

$$E_p I_p^b < \gamma^{\frac{n-m}{2m}} r_e \left(\frac{mM^2 E_b}{4n\Psi_o} \right)^{1/2} \tag{41}$$

This limit has some physical implications, since the exponent on gamma is negative of m > n. As γ goes to zero, the value of $\gamma^{(n-m)/2m}$ will become infinite, but since the magnitude of the exponent is small, this limit can be accounted for in a practical sense. For n = 3.0 and m = 3.1, the exponent is equal to –0.016129 and if $\gamma = 10^{-6}$ (the lower bound for the numerical simulations) then $\gamma^{(n-m)/2m}$ will equal only 1.25. This factor was used to predict the behavior of the simulations.

Torsional Loads

The two approximate models we used for torsional loading were essentially the same as the two bending models, but the moments of inertia for the bone and prosthesis were polar, as opposed to the bending moments of inertia used above. Planes perpendicular to the prosthesis axis were assumed to remain planar, and the rotation of prosthesis and bone was taken as equal within a plane. This led to the same formulae as in bending, with the torque substituted for the bending moment, and the polar moments of inertia substituted for bending moments of inertia. The resulting limits were given by

$$G_p I_p^p < \gamma^{2\frac{n-m}{m}} r_e \left(\frac{mT^2 G_b}{2n\Psi_o} \right)^{1/2} \tag{42}$$

with I_p^p the polar moment of inertia for the prosthesis. The limits on the set point can be given as

$$\Psi_o < \gamma^{\frac{n-m}{m}} \frac{r_o}{G_p I_p^p} \sqrt{\frac{mT^2 G_o}{2n}} \tag{43}$$

In the torsional model which corresponds to the first bending model, we took $\gamma = 1$.

FINITE ELEMENT SIMULATIONS

The elastic modulus of cancellous bone was taken as proportional to density cubed (n = 3), and the exponent on volumetric density that was used

to divide the strain energy density (m in eq. 28) was taken as 3.1, for stability considerations, and based on earlier experience.[18] The density was limited to be no greater than 1.0 or less than 0.01. The norm (or size) of an increment in density within a given time step was judged by summing up the square of each density increment, dividing by the number of remodeling elements, and taking the square root of that quantity. The same was done to compute the norm of the remodeling rate and the norm of the overall density distribution. These norms were computed only for the elements in which the density was greater than 0.01 and less than 1.0

A) Axial loading

An axisymmetric model was used. The prosthesis diameter was 15 mm, with 5 mm of cancellous bone modelled between the outer surface of the implant and the cortex, which was 5 mm thick. Axial loads were applied to the top of the prosthesis, and the bottom of the bone was fixed. All interfaces were assumed to be perfectly bonded. We assumed that the distal tip of the intramedullary stem was spherical, and the distance from the distal tip of the prosthesis to the upper level of the femur was 107.5 mm. The prosthesis extended 10 mm beyond the end of the cortex. The details of the finite element mesh are reported in a prior paper.[21]

Ten simulations were run to test the optimizing predictions in axial loading, with both the cortex and the cancellous bone allowed to remodel. Within the simulations, the prosthesis elastic moduli were chosen using a scaling procedure as detailed below. We took the elastic modulus of fully dense bone as 17 GPa, and the prosthesis moduli to be 17, 34, 85, 136, and 204 GPa. The load which is relevant to the data in table 1 is 1000 N, applied vertically as a point load to the top of the intramedullary stem. The cortical bone was fully dense ($\gamma = 1.0$) and the initial density of cancellous bone was simulated by taking $\gamma = 0.5$.

The simulation cases we used in this study were chosen to test equations 36 and 37 simultaneously. For each prosthesis elastic modulus, a limiting value of Ψ_0 was calculated from eq. 36. Six values of Ψ_0 were established so that we could test the limiting value of prosthesis stiffness, as predicted from eq. 37. Table 1 shows how the ten finite element runs in this study were used to test eq. 36, and table 2 shows how eight of these ten cases were used to test eq. 37.

B) Transverse Bending Loads

Seven three-dimensional finite element simulations were run in this study to assess the remodeling response of bone adjacent to an intramedullary

TABLE I

Remodeling cases used to test predicted limits on E_p in axial loading.

Elastic Modulus (GPa)	Upper limit on Ψo (J/m^3)	Simulation Value Above(Case No.)	Simulation Value Below(Case No.)
17	973.1	1055.8 (A1)	422.3 (A6)
34	243.3	422.3 (A2)	84.5 (A7)
85	38.9	84.5 (A3)	33.8 (A8)
136	15.2	33.8 (A4)	8.4 (A9)
204	6.8	8.4 (A5)	4.2 (A10)

stem which was loaded by a 100 in-lb transverse bending moment. The finite element model consisted of a cylindrical stem with a spherical end cap which was surrounded by bone with a cylindrical outer surface. The cylindrical portion of the stem was 100 mm long and the stem was 15 mm in diameter. The bone outer diameter was 35mm. In the model, bone extended past the stem tip a distance of 10 mm and extended proximally to the top of the stem. The finite element model incorporated the entire stem and bone (i. e. a full 360 degree model was used) so that we could check for numerical problems by comparing left and right halves of the model.

This model was generated using ADINA-IN (ADINA Engineering, Watertown, MA) and the finite element data was re-formatted for our simulation program using a translation program and a text editor.

C) Torsional Loading

Using the finite element mesh developed above for bending loads, six remodeling simulations were run using n = 3.0 and m = 3.1 as above. A 100 in-lb torque was applied through four nodal point loads at the top of the prosthesis, and limits on Ψ_o were derived using equation 48 for three values of prosthesis elastic modulus. In three finite element simulations,

TABLE II

Remodeling cases used to test predicted limits on Ψ_o in axial loading.

Value of Ψo (J/m^3)	Upper limit on E (GPa)	Simulation Value Below(Case No)	Simulation Value Above(Case No.)
422.3	25.8	17 (A6)	34 (A2)
84.5	57.7	34 (A7)	85 (A3)
33.8	91.2	85 (A8)	136 (A4)
8.4	182.5	136 (A9)	204 (A5)

the limit on Ψ_o in equation 43 was satisfied with $\gamma = 1.0$, and in three the limit on Ψ_o in equation 43 was violated with $\gamma = 10^{-6}$. Three values of prosthesis stiffness were used.

The information on the derived limits and the cases used to test these limits are summarized in table 4.

D) Transverse force effects

A transverse load on a beam produces both a bending moment and a shear stress in the beam. To assess the effect of this shear stress on the composite beam made up of remodeling bone and a prosthesis, we ran eight finite element simulations with a pure transverse load of 250N applied to the top of the prosthesis. Since we did not have an analytic model for the effect of shear stress on bone remodeling around an implant, we varied the remodeling set point from 20 to 200 J/m^3, with the prosthesis modulus taken as either 115 GPa (Titanium) or 200GPa (steel). The simulation data for these cases is summarized in Table 5.

SIMULATION SCALING AND CONVERGENCE CRITERIA

In the numerical simulations we ran, we took advantage of the simple formula for the remodeling rate equation by establishing scaling rules similar to those detailed in a prior paper[20]. In the finite element simulations, the two important equations are the finite element system of equations, KU = R, and the remodeling rule, equation 19 above. If we hold the dimensions of the model fixed, and consider scaling the load R, the finite element matrix K, and the set point Ψ_o and the simulation time t in the remodeling simulation, we can use the following scaling equations.

$$R = \beta R^s \quad K = \alpha K^s \quad \Psi_o = \eta \Psi_o^s \quad t = \mu T \tag{44}$$

Substituting these expressions into the finite element and remodeling equations shows that to use scaled variables, we need to choose scaling factors which obey equations

$$\frac{\beta^2}{\alpha} = \eta = \frac{1}{\mu} \tag{45}$$

to make the numerical simulation match the physical problem. Using these scaling relationships, we can identify physical problems which have the same solution, For example, scaling up the load by a factor of

two with everything else the same corresponds to scaling up the set point by a factor of four. The scaling factors we used in this study, and the actual (scaled) values for elastic moduli are listed in Tables 3 to 6.

Using the scaling relationships here, we can also relate the scaled rate of change to the actual rate of change using μ. Since simulation time is equal to actual time (in eq. 26) divided by μ, then the convergence criterion in simulation time scales as follows:

$$\left[\sum_{e=1}^{N}\left(\frac{d\gamma_e}{dT}\right)^2\right]^{1/2} < \epsilon_s \Rightarrow \left[\sum_{e=1}^{N}\left(\frac{d\gamma_e}{dt}\right)^2\right]^{1/2} < \frac{\epsilon_s}{\mu} = \epsilon_{act} \qquad (46)$$

with ϵ_s the convergence criterion for the simulation time. The "actual" time in eq. (26) is scaled so that the rate coefficient is unity so the convergences are relative. However, the numerical values for convergence are all quite small.

RESULTS

If an optimization method is used to predict bone remodeling in general, two comparisons should be made, but in this study we can make only one, between the simplified optimization model and the behavior of the remodeling simulation. The other comparison, between the simulation results and the remodeling which occurs in vivo, remains to be explored fully.

In the cases where axial, torsional, and transverse bending loads are studied, the optimization predictions correctly predict general trends,

TABLE III

Simulation scaling and convergence data for axial loading.

Case	Ψ_o (actual)	α	E_p(sim)	E_b (sim)	μ	ϵ_{act}
A1	1055.8	6,800	2.5	2.5	473.5	4.33×10^{-5}
A2	422.3	17,000	2.0	1.0	1183.8	23.5×10^{-6}
A3	84.5	84,967	1.0	0.2	3410.0	3.48×10^{-7}
A4	33.8	212,419	0.64	0.08	14,792.8	1.65×10^{-7}
A5	8.4	854,735	0.24	0.02	59,523.8	5.56×10^{-10}
A6	422.3	17,000	1.0	1.0	1183.8	9.61×10^{-7}
A7	84.5	84,967	0.4	0.2	3410.0	1.43×10^{-6}
A8	33.8	212,419	0.4	0.08	14,792.8	1.81×10^{-7}
A9	8.4	854,735	0.16	0.02	59,523.8	1.22×10^{-7}
A10	4.2	1,709,470	0.12	0.01	119,047.6	5.57×10^{-8}

TABLE IV

Cases used to test predictions in transverse bending.

Case number	Ψ_o (actual) (J/m^3)	α	E_p (GPa)	E_p(sim)	E_b(sim)	Final rate of change
B1(*)	2500	200	85	425	85	4.043×10^{-6}
B2(*)	1000	500	115	230	34	5.09×10^{-6}
B3(**)	2500	200	115	575	85	1.775×10^{-6}
B4(***)	5000	100	115	1150	170	5.49×10^{-6}
B5(*)	500	1000	200	200	17	3.162×10^{-6}
B6(**)	1000	500	200	400	34	3.483×10^{-6}
B7(***)	2500	200	200	1000	85	1.485×10^{-6}

Cases in which bone mintenance is predicted by both models are indicated with (*). Cases which were predicted to resorb by the first model and maintain bone by the second model are indicated with (**). Cases which were predicted to resorb by both models are indicated by (***).

and they seem useful as a way to predict the behavior of the large-scale simulations. The large-scale simulations behaved very well, and they produced results which qualitatively matched what would be expected from bone remodeling in vivo.

The axial loading results are shown in Figures 6 and 7. These figures show that the lack of bone adjacent to the implant, predicted by the simplified optimization results, actually occurrs in the simulation. The cases in Figure 6 all use parameter values which should cause zero bone density around the implant, and the results are largely confirmed. In two cases, bone remained around the implant, but at a small density. Figure 7 shows cases in which bone was predicted to remain around the implant, and this was confirmed in all cases.

TABLE V

Cases used to test predictions in torsion.

case	Ψ_o (actual) (J/m^3)	α	E_p (GPa)	E_p(sim)	E_b(sim)	Final remodeling rate
T1	15000	333.33	85	2250	510	1.716×10^{-6}
T2	4500	111.11	85	765	153	1.397×10^{-5}
T3	4500	111.11	115	1035	153	5.253×10^{-6}
T4	2000	250	115	460	68	2.093×10^{-5}
T5	2000	250	200	800	68	1.097×10^{-5}
T6	800	625	200	320	27.2	8.466×10^{-6}

TABLE VI

Cases studied using a 250 newton transverse load.

case	Ψ_o (actual) (J/m^3)	α	E_p(GPa)	E_p(sim)	E_b(sim)	Final remodeling rate
S1	20	25000	115	4.6	0.68	1.454×10^{-7}
S2	50	10000	115	11.5	1.7	4.492×10^{-7}
S3	100	5000	115	23.0	3.4	6.608×10^{-7}
S4	200	2500	115	46.0	6.8	7.274×10^{-7}
S5	20	25000	200	8	0.68	1.272×10^{-7}
S6	50	10000	200	20	1.7	3.952×10^{-7}
S7	100	5000	200	40	3.4	3.547×10^{-7}
S8	200	2500	200	80	6.8	1.680×10^{-7}

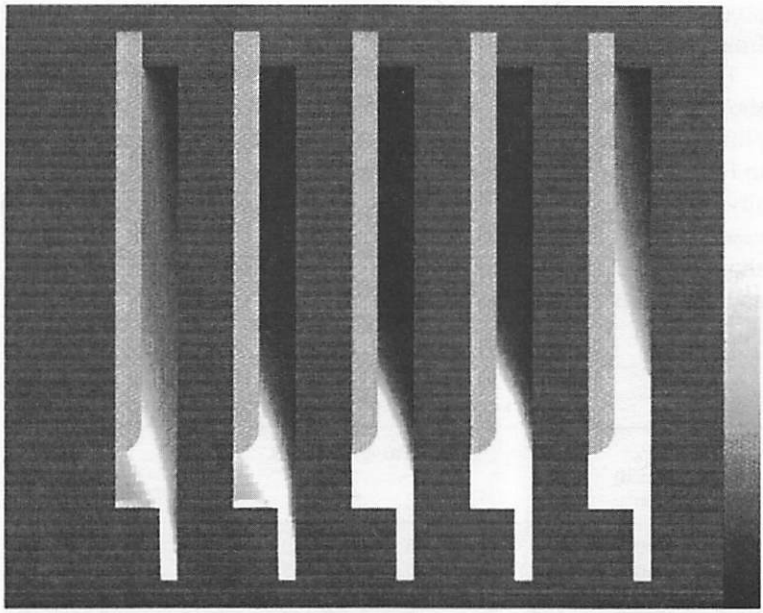

FIGURE 6 Density results for cases A1 (leftmost) to A5 (rightmost). The color bar on the right indicates the density from zero (bottom, black) to 1.0 (top, white). The dramatic bone loss is as predicted by the optimization approach. (See color plate I)

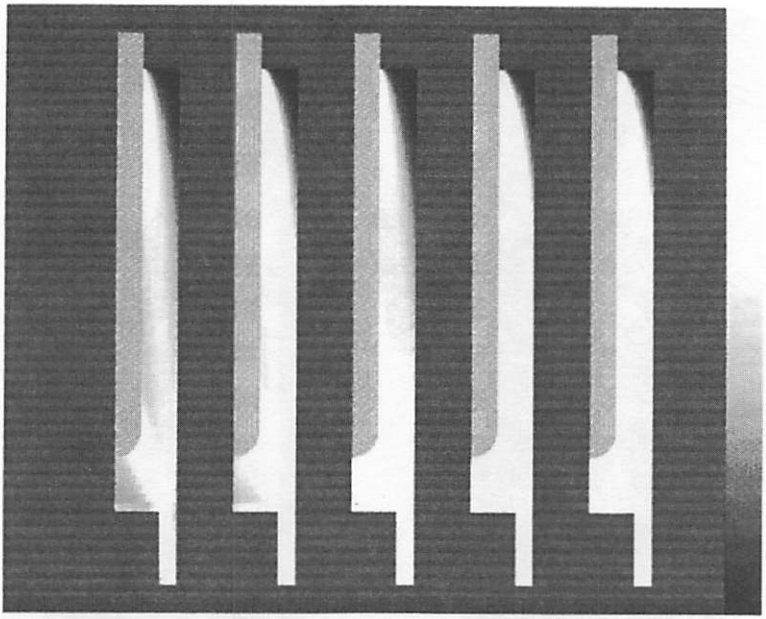

FIGURE 7 Density results for cases A6 (leftmost) to A10 (rightmost). As in Figure 1, the color bar on the right indicates the density from zero (bottom, black) to 1.0 (top, white). Bone maintenance is as predicted by the optimization approach. (See color plate II)

In cases where bone remained around the implant, the density distributions in axial loading showed low density in the proximal exterior corner, and high bone density below the implant. This increased bone density under the implant was similar in all cases. In the lower modulus cases, regions of low bone density occurred near the implant in the lower third of the stem.

The bending moment cases are shown in Figure 8. These are 90 degree sectors of the full 360 degree model, with the cuts oriented in the plane of the bending moment, and perpendicular to it. The bone density in the plane perpendicular to the moment is at the allowed simulation minimum, and the bone in the plane of the moment seems to obey the predictions of the optimization predictions. Where the optimization model for fully dense bone predicts resorption, but the optimization model for very low density predicts bone to remain, there is bone in parallel to the implant, but the density is below 1.0. In cases where both bending optimization predictions predict no bone to remain, the simulations show densities at the low numerical limit.

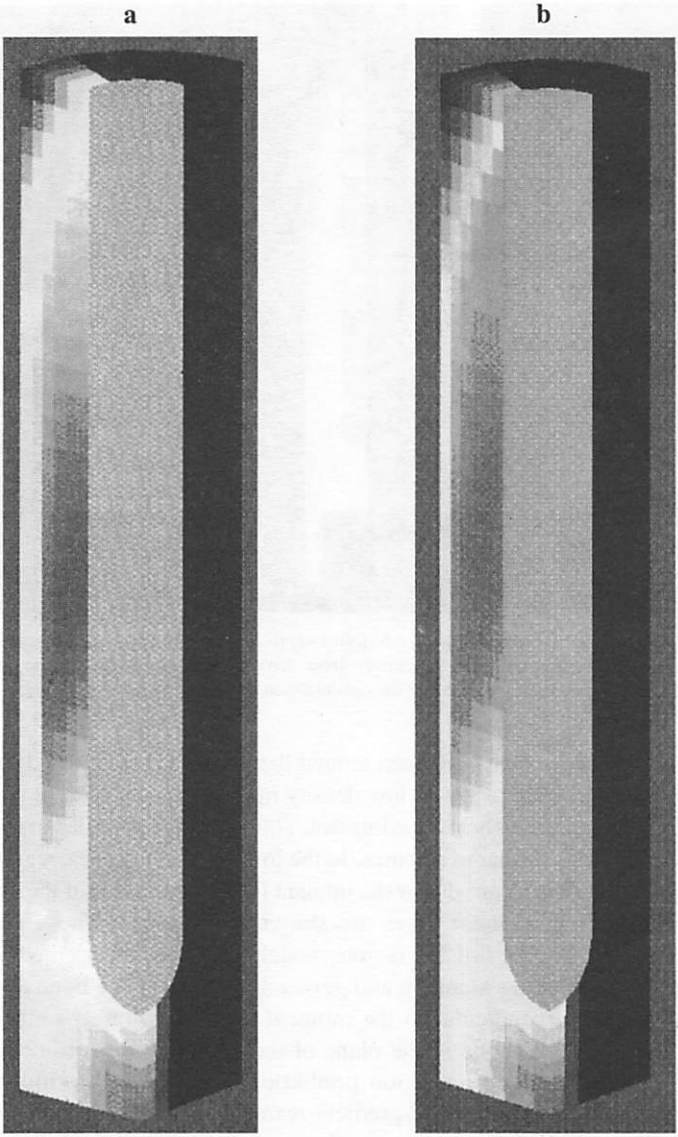

FIGURES 8a and 8b Density results for cases B1(left) and B2 (right). Bone remains in parallel to the implant when predicted, but regions of low density are apparent near the mid-shaft of the implant in that case. Bone forms primarily in the plane of bending. The density is shown by colors according to the scale shown in figure 6. (See color plate III)

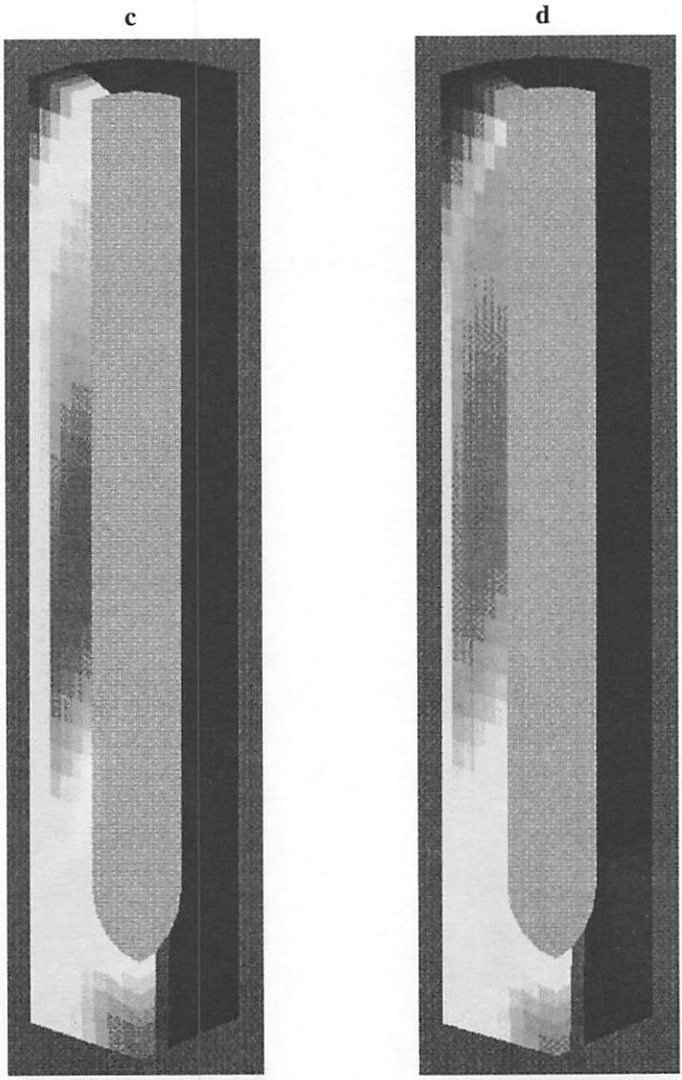

FIGURES 8c and 8d Density results for cases B3 (left) and B4 (right). The density is shown by colors according to the scale shown in Figure 6. (See color plate IV)

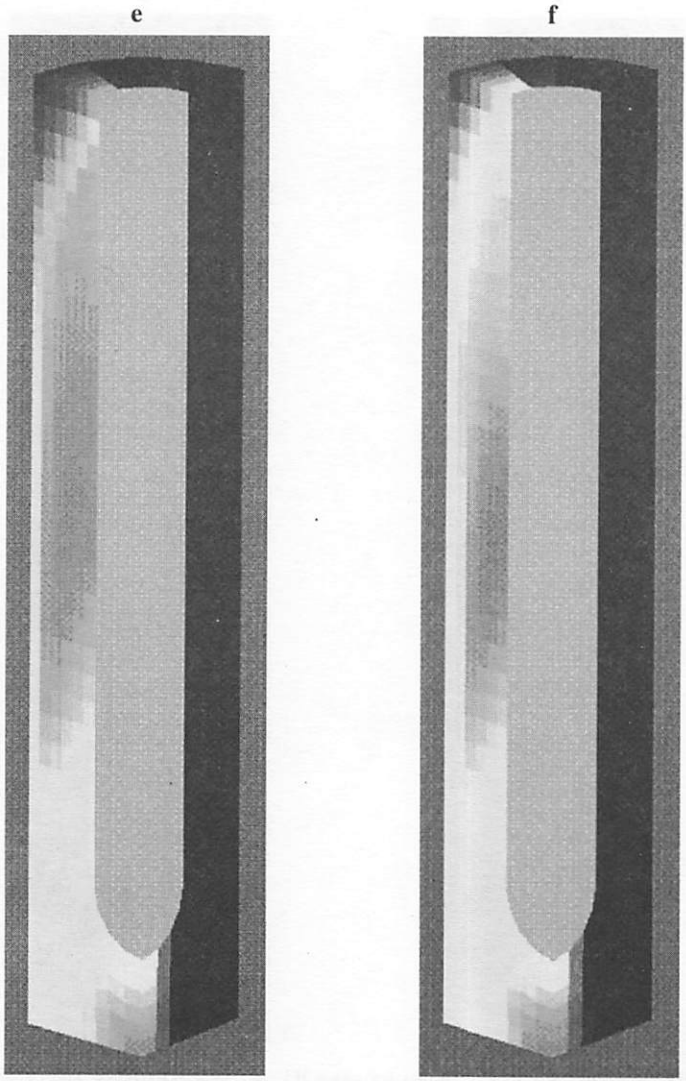

FIGURES 8e and 8f Density results for cases B5 (left) and B6 (right). The density is shown by colors according to the scale shown in Figure 6. (See color plate V)

g

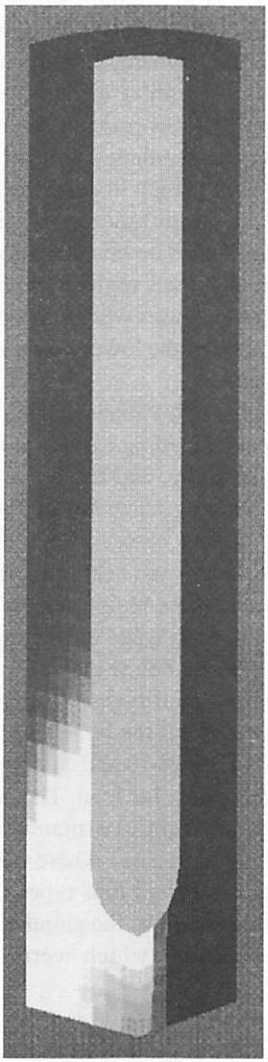

FIGURE 8g Density results for case B7. The density is shown by colors according to the scale shown in Figure 6. (See color plate VI)

In the bending moment cases where bone remains around the implant, the bone density is highest away from the implant, and the bone density adjacent to the implant is quite low. This low density extends along the implant toward the lower end, where, in both cases, the bone density is very high. This high density similar to that found around the implant ends in axial loading cases. However the bone density directly under the axis of the implant is low in bending cases, whereas the bone density under the axis of the implant is high in axial loading cases.

In torsional loading, the optimization predictions were borne out by the finite element calculations. The bone density patterns showed bone loss in the most proximal lateral regions even when bone remained around the implant, and in the cases where the optimization method predicted no bone, the bone was at the lower numerical limit adjacent to the implant, as shown in Figure 9.

The bone density patterns in torsional loading cases show some similarities to the patterns in axial loading cases, but the density distributions in torsion are axially symmetric, and the bone density distributions in bending are high in the bending plane but low near the neutral axis. In both the torsional and bending cases, when bone remains around the implant, regions of low density exist near the implant surface in the middle range of the implant, and these regions extend over much of the middle of the implant. Also, in both types of loading cases also, regions of low density were found directly below the axis of the implant.

Transverse loading yielded density distributions which were similar to a transverse bending moment, but the bone density at the neutral axis of the structure was not zero. Figures 10 and 11 shows the bone density distributions in the cases for a pure side load. The density near the plane of the neutral axis is higher adjacent to a titanium implant, compared to steel, and the density is higher in cases where the set point is lower.

The final remodeling rates for all four types of loading are shown in Tables 3 to 6, and are quite small. In the simulation code, a stability test was conducted on the solutions which were obtained, and all were graded as stable.

DISCUSSION

This paper reviews some recent developments in mechanical models for bone remodeling. Other approaches to mechanical effects in bone

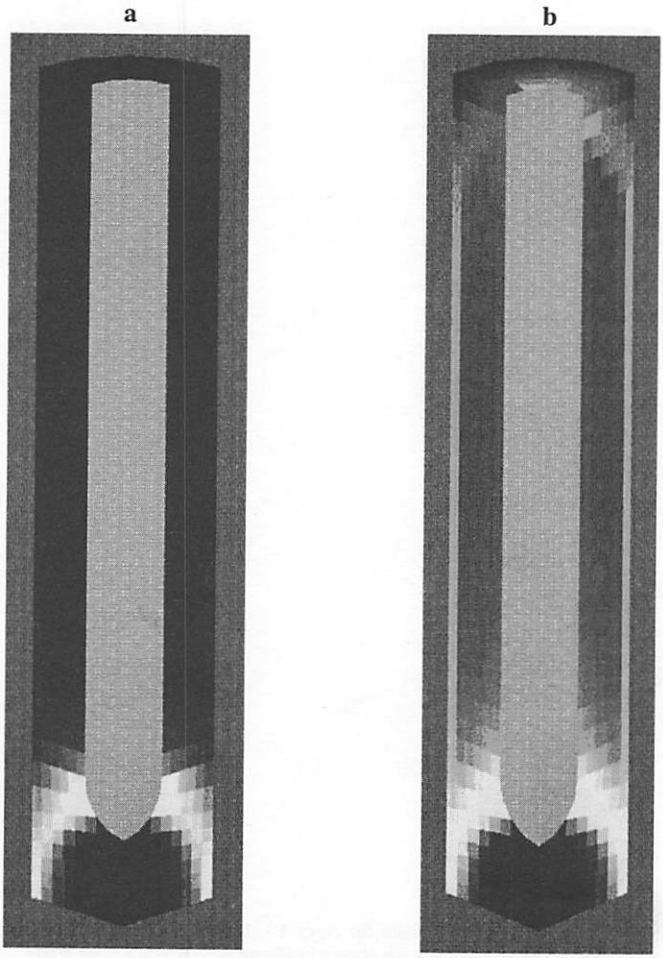

FIGURES 9a and 9b Density Results for cases T1 (left) and T2 (right). Bone remains in parallel with the implant where predicted, and the distribution is circumferential. The density is shown by colors according to the scale shown in Figure 6. (See color plate VII)

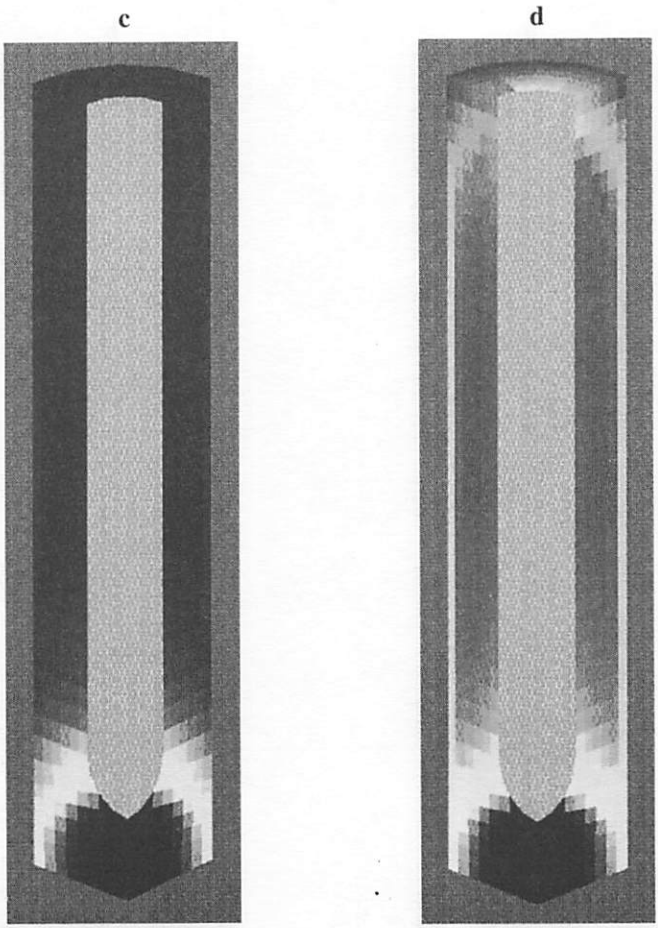

FIGURES 9c and 9d Density Results for cases T3 (left) and T4 (right). The density is shown by colors according to the scale shown in Figure 6. (See color plate VIII)

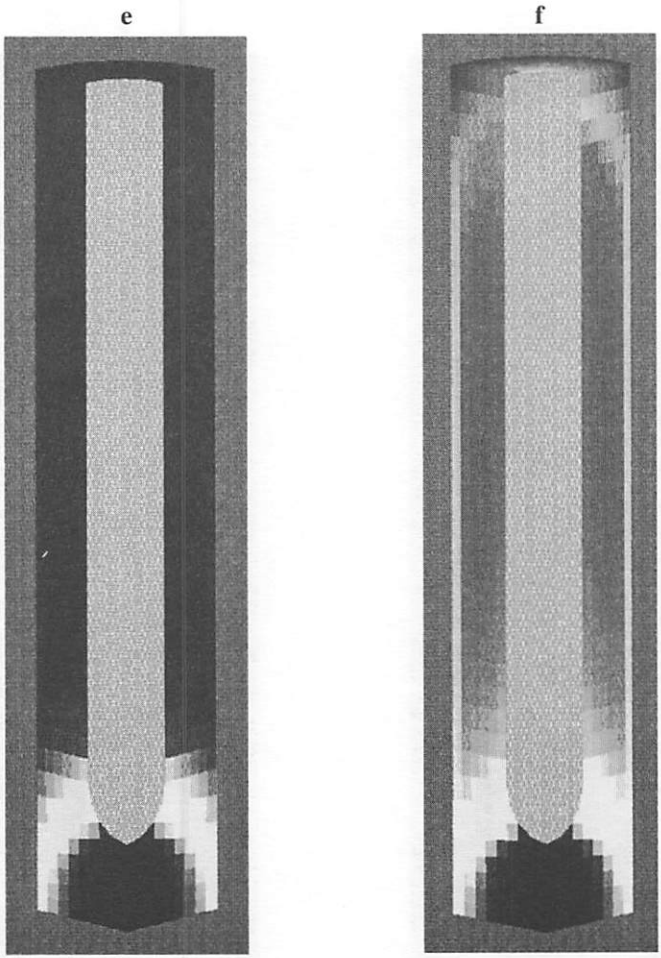

FIGURES 9e and 9f Density Results for cases T5(left) and T6 (right). The density is shown by colors according to the scale shown in Figure 6. (See color plate IX)

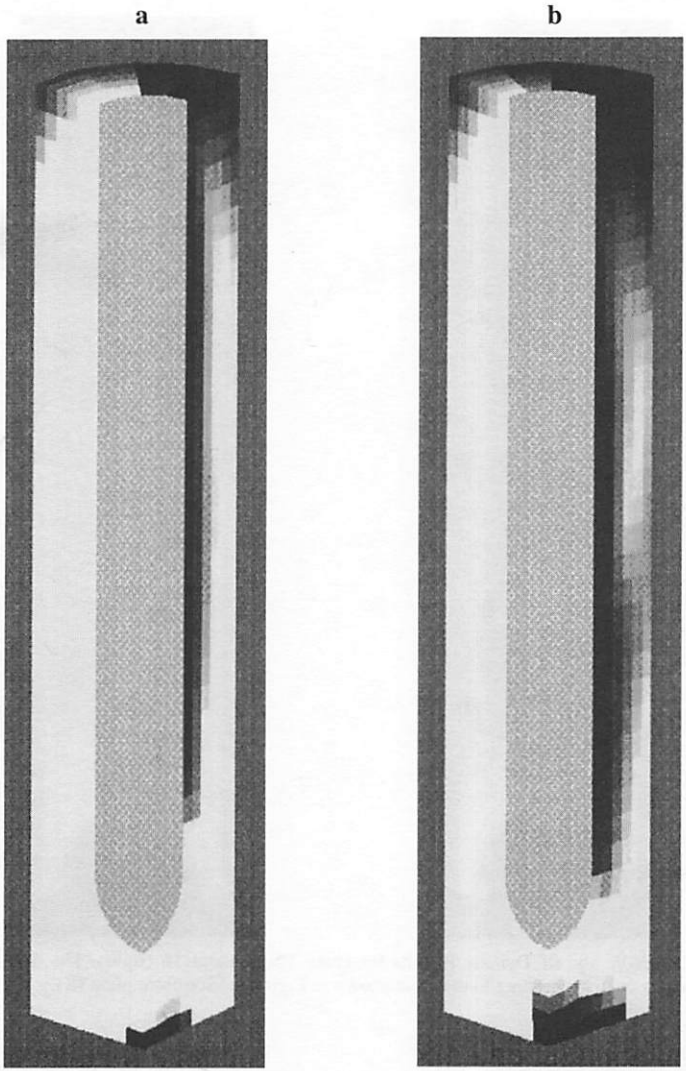

FIGURES 10a and 10b Density Results for cases S1 (left) and S2 (right). Bone remains in the neutral plane of bending, and more bone is apparent as the set point is raised. More bone is apparent than would be predicted from a 1000 N axial load, and more bone is apparent around a Titanium implant than around a Steel implant The density is shown by colors according to the scale shown in Figure 6. (See color plate X)

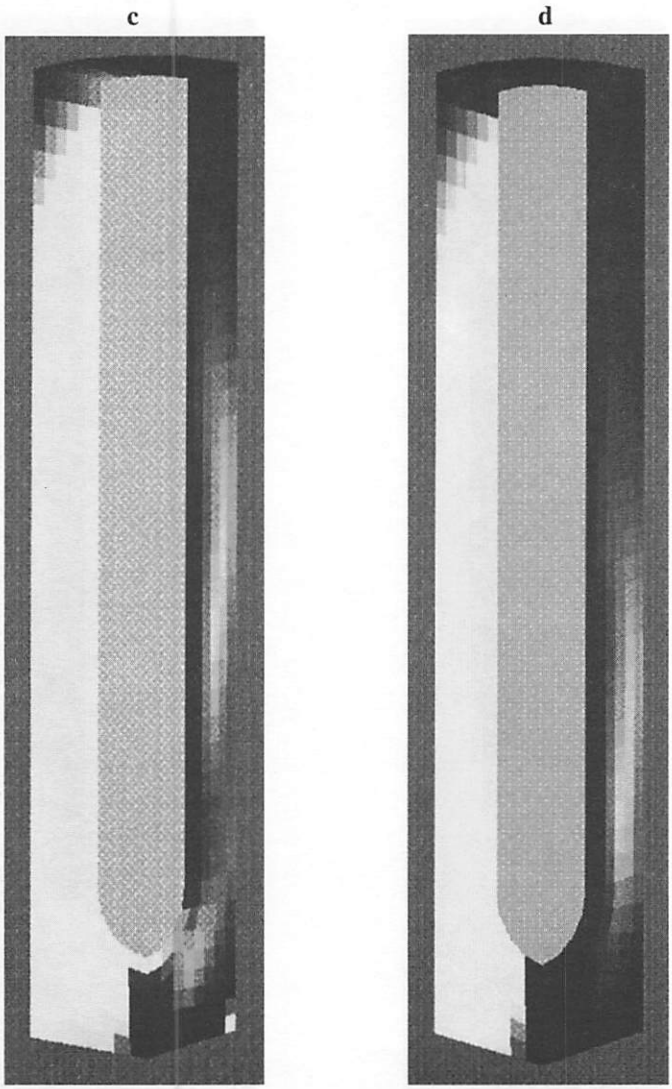

FIGURES 10c and 10d Density Results for cases S3 (left) and S4 (right). The density is shown by colors according to the scale shown in Figure 6. (See color plate XI)

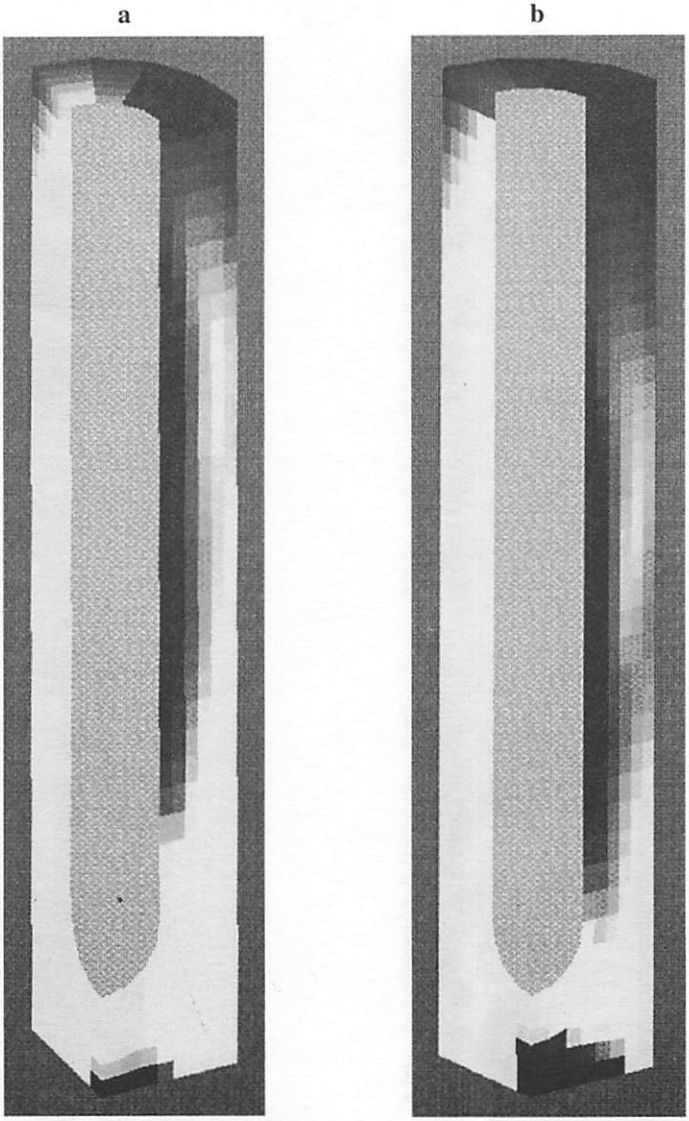

FIGURE 11a and 11b Density Results for cases S5 (left) and S6 (right). The density is shown by colors according to the scale shown in Figure 6. (See color plate XII)

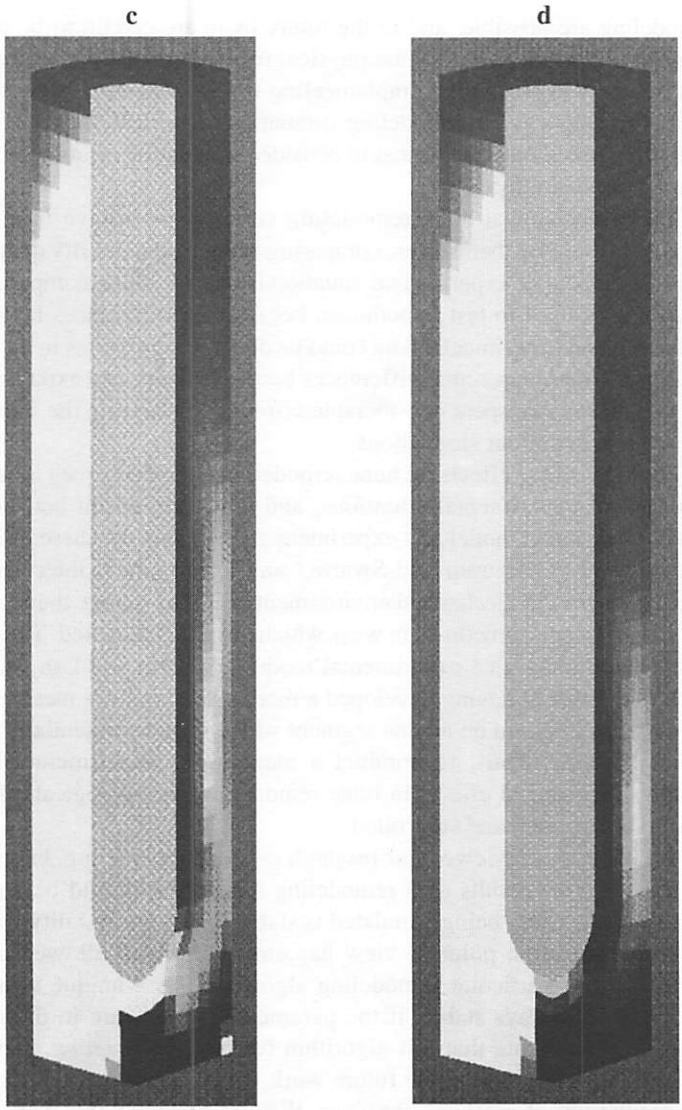

FIGURES 11c and 11d Density Results for cases S7 (left) and S8 (right). The density is shown by colors according to the scale shown in Figure 6. (See color plate XIII)

remodeling are possible, and in the future there are certain to be more accurate characterizations of the physical relationships we have used in this paper. However, when implementing more accurate relationships, and comparing a given remodeling simulation to clinical or experimental results, two issues are critical to consider: simulation robustness, and non-mechanical effects.

Unless mechanical bone remodeling simulations behave in a predictable fashion by themselves, comparing a calculated density distribution to a clinical or experimental situation is useless. Such comparisons could not be used to test hypotheses, because the differences between calculated and experimental data could be due to irregularities in the calculations, rather than actual differences between theory and experiment. For this reason, we spent considerable effort characterizing the stability and uniqueness of our simulations.

Non-mechanical effects on bone remodeling are clearly seen in many clinical and experimental situations, and any comparison between a purely mechanical model and experiment should consider these effects. As reviewed by Bertram and Swartz,[5] any experimental intervention which changes the mechanical environment will also change the biological environment, sometimes in ways which are not anticipated. The success of the turkey ulna experimental model by Rubin and Lanyon[53] is partly the result of having developed a model which allows mechanical effects to be imposed on a bone segment which is under essentially normal conditions. Thus, to conduct a meaningful experiment which explores mechanical effects in bone remodeling, the biological effects need to be explored and controlled.

This paper has reviewed our research on bone remodeling, based on the idea that the results of a remodeling simulation should be stable, because the process being simulated is stable. From the stability analysis an optimization point of view has emerged which allowed us to prove that our particular remodeling algorithm has a unique solution and that it is always stable, if the parameters we use are in the right range. We anticipate that this algorithm for bone remodeling, and the analysis behind it, will allow future work which can make more accurate predictions of mechanical effects. We also hope that this work will lead to simulations which account for biological changes in bone, so that by exploring what is explained by these simulations (and what is not) we can gain still better insights into bone changes in disease and around total joint implants.

Acknowledgements

This research was supported in part by Pittsburgh Supercomputing Center grant Number 1 P41 RR06009 from the NIH Netional Center for Research Resources, in part by the grant Ricerca Finalizzata of Italian Ministery of Health, del. CIPE 13/10/92 entitled "Studio dei fattori che governano il fenomeno di adattamento funzionale del tessuto osseo ai carichi meccanici", and in part by a gift from Wright Medical Technology, Inc.

TIMOTHY P. HARRIGAN,* FRANCES B. BIEGLER and JEFFREY D. REUBEN
Department of Orthopedic Surgery
University of Texas Health Sciences Center at Houston
6431 Fannin, Suite 6.154
Houston, Texas, 77030

References

1. Bathe, K. J.: Finite Element Procedures In Engineering Analysis, Prentice-Hall, Englewood Cliffs, NJ (1982).
2. Beaupré, G. S., Orr, T. E., Carter, D. R.: An Approach for Time-Dependent Bone Modeling and Remodeling—Theoretical Development, J. Orthopaedic Research **8**, 651–661 (1990).
3. Beaupré, G. S., Orr, T. E., Carter, D. R.: An Approach for Time-Dependant Bone Modeling and Remodelling—Application: A Preliminary Remodelling Simulation, J. Orthopaedic Research **8**, 662–670 (1990).
4. Biewener, A. A., Bertram, J. E. "Skeletal strain patterns in relation to exercise training during growth." Journal of Experimental Biology. **185**, 51–69, 1993 Dec.
5. Bertram, J. E., Swartz, S.M. "The 'law of bone transformation': a case of crying Wolff?" Biological Reviews of the Cambridge Philosophical Society. **66**(3), 245–73, 1991 Aug.
6. Carter, D. R., Hayes, W. C. The Compressive Behavior of Bone as a Two-Phase Porous Structure, J. Bone and Joint Surgery **59A**, 954–962 (1977).
7. Carter, D. R., Fyhrie, D. P., Whalen, R. T.: Trabecular Bone Density and Loading History: Regulation of Connective Tissue Biology by Mechanical Energy. J. Biomechanics **20**, 785–794 (1987).
8. Carter, D. R.: Mechanical Loading History and Skeletal Biology, J. Biomechanics **20**, 1095–1109 (1987).
9. Cowin, S. C.: Mechanical Modeling of the Stress Adaptation Process in Bone. Calcif. Tiss. Int **36**(suppl 1), S98–S103 (1984).
10. Cowin, S. C. "Wolff's law of trabecular architecture at remodeling equilibrium. Journal of Biomechanical Engineering. **108**(1), 83–8, 1986 Feb.

* Corresponding author. Tel.: 713-500-7004 FAX: 713-500-6999
E-mail: tharriga@ortho1.med.uth.tmc.edu

11. Cowin, S. C.: Bone Remodelling of the Diaphyseal Surface By Torsional Loads: Theoretical Predictions. J. Biomechanics **20**, 1111–1120 (1987).
12. Cowin, S. C.: Periosteal and Endosteal Control of Bone Remodelling Under Torsional Loading, Trans. Orth. Res. Soc. **16**, 11 (1991).
13. Frost, H. M. "Vital Biomechanics: Proposed General Concepts for Skeletal Adaptations to Mechanical Usage", Calc. Tiss. Int. **42**, 145–156 (1988).
14. Harrigan, T. P., Carter, D. R., Mann, R. W., Harris, W. H.: The Influence of Apparent Density and Trabecular Orientation on the Elastic Modulus of Cancellous Bone, Tran. Orthopaedic Research Society **6**, 277 (1981).
15. Harrigan, T. P., Mann, R. W.: Characterization of Microstructural Anisotropy in Orthotropic Materials Using a Second Rank Tensor, J. Materials Science **19**, 761–767 (1984).
16. Harrigan, T. P. "Bone Compliance and its Influence on Human Hip Joint Lubrication", Doctoral Thesis, Mass. Inst. of Tech. (1985).
17. Harrigan, T. P., Jasty, M., Mann, R. W., Harris, W. H.: Limitations on the Continuum Assumption in Cancellous Bone, J. Biomechanics **21**(4), 269–275 (1988).
18. Harrigan, T. P., Hamilton, J. J.: An Analytical and Numerical Study of the Stability of Bone Remodelling Theories: Dependance on Microstructural Stimulus, J. Biomechanics, **25**(5), 477–488 (1992).
19. Harrigan, T. P., Hamilton, J. J.: Optimality Conditions for Finite Element Simulation of Adaptive Bone Remodelling, Int. J. Solids Structures **29**(23), 2897–2906 (1992).
20. Harrigan, T. P., Hamilton, J. J.: Finite Element simulation of Adaptive Bone Remodelling: A Stability Criterion and A Time Stepping Method, International Journal for Numerical Methods in Engineering, **36**, 837–854 (1993).
21. Harrigan, T. P., Hamilton, J. J.: Bone Remodeling Adjacent to Total hip Replacements: A Naturally Occurring Material Design Problem, Journal of Computer-Aided Materials Design **1**, 27–40 (1993).
22. Harrigan, T. P., Hamilton, J. J.: Bone Remodeling and Structural Optimization, Journal of Biomechanics, **27**(3), 323–328 (1994).
23. Harrigan, T. P., Hamilton, J. J.: Necessary and Sufficient Conditions for Global Stability and Uniqueness in Finite Element Simulations of Adaptive Bone Remodeling, International Journal of Solids and Structures, **31**(1), 97–107 (1994).
25. Harrigan, T. P., Odgaard, A., Reuben, J. D. "Comparison Between a Two-State Markov Model and Intercept Measurements Shows Small-Scale Structural Order, ASME Summer Bioengineering Conference, Beaver Creek, Colorado (1995).
26. Harrigan, T. P., Hamilton, J. J., Reuben, J. D., Toni, A., Viceconte, M.: Bone Remodeling Adjacent to Total Hip Replacements: An Optimal Structures Approach, Biomaterials, **17**, 223–232 (1996).
27. Hart, R. T., Davey, D. T.: Theories of Bone Modelling and Remodelling, In: Bone Mechanics, Edited by SC Cowin, Boca Raton, FL, CRC Press, pp. 253–277 (1989).
28. Hollister, S. J., Brennan, J. M., Kikuchi, N. A homogenization sampling procedure for calculating trabecular bone effective stiffness and tissue level stress", Journal of Biomechanics. **27**(4), 433–44, 1994 Apr.
29. Huiskes, R., Weinans, H., Grootenboer, H. J., Dalstra, M., Fudala, B., Sloof, T. J.: Adaptive Bone Remodelling Theory Applied to Prosthetic Design Analysis. J. Biomechanics **20**, 1135–1150 (1987).
30. Huiskes, R.: Stress Patterns, Failure Modes, and Bone Remodelling, Chapter 24 in "Non-Cemented Total Hip Arthroplasty" Edited by R. Fitzgerald, Jr., Raven Press, New York (1988).
31. Huiskes, R., Weinans, H. E., van Reitbergen, B.: The Relationship Between Stress Shielding and Bone Resorption Around Total Hip Stems and the Effects of Flexible Materials, CORR **274**, 124 (1992).

32. Jacobs, C. R., Levenston, M. E., Beaupre, G. S., Simo, J. C. Carter, D.R. Numerical instabilities in bone remodeling simulations: the advantages of a node-based finite element approach., Journal of Biomechanics. **28**(4), 449–59, 1995 Apr.
33. Levenston, M. E., Beaupre, G. S., Jacobs, C. R., Carter, D.R. The role of loading memory in bone adaptation simulations. Bone. **15**(2), 177–86, 1994 Mar–Apr.
51. Lancaster, P., Tismenetsky, M. *The Theory of Matrices*, Academic Press, Orlando, FL (1985).
52. McMahon, T. A. "Muscles, Reflexes, and Locomotion", Princeton University Press, Princeton, NJ (1984).
53. Rubin, C. T., Lanyon, L.E.: Osteoregulatory Nature of Mechanical Stimuli: Function as a Determinant for Adaptive Remodelling in Bone, J. Orthopaedic Research **5**(2), 300–310 (1987).
54. Weinans, H., Huiskes, R., Grootenboer, H. J. Convergence and Uniqueness of adaptive Bone Remodelling, Trans. Orthopaedic Research Society **14**, 310 (1989).
55. Weinans, H., Huiskes, R., Grootenboer, H. J. Numerical Comparisons of Strain-Adaptive Bone Remodelling Theories, Trans. First World Congress of Biomechanics, **II**, 75 (1990).
56. Weinans, H., Huiskes, R., Grootenboer, H. J.: "The Behavior of Adaptive Bone-Remodeling Simulation Models", J. Biomechanics **25**, 1425–1441 (1992).
57. Wolff, J. L.: The Law of Bone Remodelling, Translated by P. Maquet and R. Furlong, Berlin, Springer-Verlag (original Publication 1892) (1976).